Wind turbine rotor blade monitoring using digital image correlation: a comparison to aeroelastic simulations of a multi-megawatt wind turbine

2014 J. Phys.: Conf. Ser. 524 012064

(http://iopscience.iop.org/1742-6596/524/1/012064)

Wind turbine rotor blade monitoring using digital image correlation: a comparison to aeroelastic simulations of a multi-megawatt wind turbine

J Winstroth[1], L Schoen[2], B Ernst[1] and J R Seume[1]

[1]ForWind - Center for Wind Energy Research, Leibniz Universität Hannover,
Institute of Turbomachinery and Fluid Dynamics (TFD), Appelstr. 9, 30167 Hanover, DE
[2]Senvion SE, Albert-Betz-Straße 1, 24783 Osterrönfeld, DE

E-mail: winstroth@tfd.uni-hannover.de

Abstract. Optical full-field measurement methods such as Digital Image Correlation (DIC) provide a new opportunity for measuring deformations and vibrations with high spatial and temporal resolution. However, application to full-scale wind turbines is not trivial. Elaborate preparation of the experiment is vital and sophisticated post processing of the DIC results essential. In the present study, a rotor blade of a 3.2 MW wind turbine is equipped with a random black-and-white dot pattern at four different radial positions. Two cameras are located in front of the wind turbine and the response of the rotor blade is monitored using DIC for different turbine operations. In addition, a Light Detection and Ranging (LiDAR) system is used in order to measure the wind conditions. Wind fields are created based on the LiDAR measurements and used to perform aeroelastic simulations of the wind turbine by means of advanced multibody codes. The results from the optical DIC system appear plausible when checked against common and expected results. In addition, the comparison of relative out-of-plane blade deflections shows good agreement between DIC results and aeroelastic simulations.

1. Introduction

The rated power of a wind turbine correlates with the diameter of the rotor. Over the last 30 years, commercial wind turbines have evolved from approximately 10 m rotor diameter and a rated power of 50 kW into today's multi-megawatt class with rotor diameters exceeding 150 m and rated power of well above 6 MW. This development has produced light, slender, and flexible structures, for which the aeroelastic characteristics of the turbine become increasingly important for fatigue strength and overall performance.

Sophisticated design tools, which have been calibrated and validated against experimental data, are needed in order to optimize energy production, to ensure a long life time with low maintenance cost and high operational reliability and safety. However, experimental data from full-scale wind turbines often focuses on the integral moments and forces captured during measurements for certification. Detailed measurements of blade deformations are rare and quite hard to gather because of the large scales involved. Recent advances in digital camera technology make optical techniques an interesting and promising tool for small-scale and full-scale wind-turbine testing. In [1] a wind turbine rotor with 40 m diameter and a nacelle height of 70 m was monitored during operation at 50 discrete points scattered across the rotor and the tower using

a point tracking algorithm. The same optical technique was later extended to even larger scales by [2]. They analyzed a 2.5 MW wind turbine with an 80 m rotor diameter at 33 discrete points. Later, [3] analyzed the recorded data from the field-test by using an operational modal analysis algorithm and compared the results against data from strain gauges, laser interferometry, and the literature.

The present project aims to apply an optical Digital Image Correlation (DIC) measurement technique for 3D deformation and vibration measurements of the rotor blades during operation in the field. It is supposed to provide a superior spatial resolution and an improved accuracy compared to the aforementioned point-tracking method. A common DIC setup on a wind turbine is shown in Figure 1. The two cameras (blue) are at a fixed position on the ground approximately 205 m in front of the wind turbine. The distance between the cameras is about 105 m. Synchronization of the cameras is achieved by an external trigger pulse. Each camera monitors the entire rotor, but from a different perspective. A random black-and-white speckle pattern is applied on the pressure side of the rotor blades. The areas tracked during operation are the areas where the random pattern is applied.

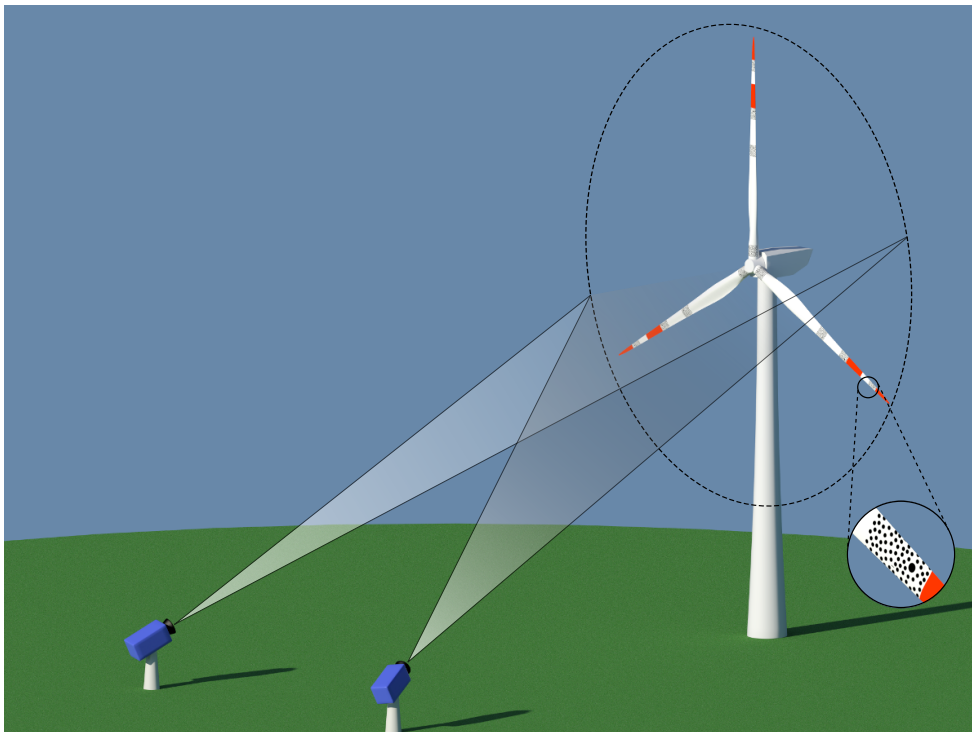

Figure 1. Schematic of a camera setup in front of a full-scale wind turbine. The magnified cutout near the blade tip shows the random black-and-white pattern on the pressure side.

The commercial software VIC-3D, a three-dimensional DIC software by Correlated Solutions, is used for the present investigations. The technique has widespread use in the fields of structural mechanics and dynamics [4]. However, its application is generally limited to small measurement volumes and tests are usually conducted in laboratories under controlled conditions. The objective of the present project is to apply DIC to a large measurement volume, namely a 3.2 MW wind turbine, demonstrate feasibility, and to measure out-of-plane (OoP), in-plane (IP), and torsional deflection of the rotor blades during operation.

Prior to the present study, the accuracy of DIC, when applied to wind turbines, has been evaluated experimentally on a scaled model by the authors [4]. Their results show very good

agreement between DIC, strain gauge, and laser distance measurements. Later, their work was extended based on computer simulations. In [5] a virtual 3D model of a multi-megawatt class wind turbine was created and animated in a 3D modeling environment. The rendered images of this virtual turbine were processed with DIC for different operational and deformational stages. Since the exact deformations of the wind turbine model were known, they could be directly compared to the results from DIC. These results also show good agreement between the superimposed deformations on the virtual model and the DIC results based on the rendered images.

2. Digital Image Correlation

In the present work the term Digital Image Correlation is used as a general term to refer to an optical measurement technique that combines methods from photogrammetry, computer vision, image registration, and sub pixel interpolation. It can be used to measure shape, motion, deformation, and local surface strain. Common setups are based on two or more digital cameras in a stereoscopic setup and can record data in all three dimensions. The stereovision system needs to be modeled and calibrated for measurements in 3D. A pinhole camera model is used to derive the well-known collinearity equations

$$x_s = x_0 + f\frac{R_{11}(X_W - X_0) + R_{21}(Y_W - Y_0) + R_{31}(Z_W - Z_0)}{R_{13}(X_W - X_0) + R_{23}(Y_W - Y_0) + R_{33}(Z_W - Z_0)} + \Delta x \tag{1a}$$

$$y_s = y_0 + f\frac{R_{12}(X_W - X_0) + R_{22}(Y_W - Y_0) + R_{32}(Z_W - Z_0)}{R_{13}(X_W - X_0) + R_{23}(Y_W - Y_0) + R_{33}(Z_W - Z_0)} + \Delta y \tag{1b}$$

which describe the projection of a point $\boldsymbol{P}$ from world coordinates (X_W, Y_W, Z_W) onto the sensor plane (x_s, y_s). Here $R_{11}, R_{12}, R_{13}, R_{21}, R_{22}, R_{23}, R_{31}, R_{32}$, and R_{33} are the elements of a 3×3 rotation matrix describing the ϕ, β, and γ rotation between the world and the camera coordinate system. The translation between world and camera system is provided by X_0, Y_0, and Z_0. The location of the principal point on the sensor plane is (x_0, y_0) and the focal length of the pinhole system is f. Finally, the terms Δx and Δy define an arbitrary lens distortion model.

A common approach for calibration is to take a series of images of a planar calibration target with equidistant points. The location of each point in every image can be extracted and used to solve Eq. 1 in a least-squares sense to estimate the intrinsic $(f, x_0, y_0, \Delta x, \Delta y)$ and the extrinsic $(X_0, Y_0, Z_0, \phi, \beta, \gamma)$ camera parameters in a process called bundle adjustment [6]. The transformation between camera 1 and camera 2 must also be known for a complete calibration of a stereovision system. Otherwise, stereo triangulation between both cameras, which is needed to recover the third dimension lost during the imaging process, is not possible (cf. Figure 2 right). The transformation can be estimated using bundle adjustment if one synchronized image of the calibration target from both cameras is available [7].

A correspondence problem between two images, of the same scene but from different positions, must be solved before the triangulation of a 3D point $\boldsymbol{P}$ in the scene is possible. This correspondence problem becomes significantly more accessible if the scene features a non-repetitive, isotropic, and high-contrast pattern. Therefore, a random black-and-white texture or speckle pattern is usually applied to the surface under investigation. For such speckle patterns, corresponding points in both images can be found by assigning unique signatures to image sections in image 1 and finding the matching signatures in image 2. These image sections are called subsets (cf. Figure 2 left). Each subset is assigned a unique signature based on the gray values or pixel values of the subset. A correlation function, the so-called normalized sum of

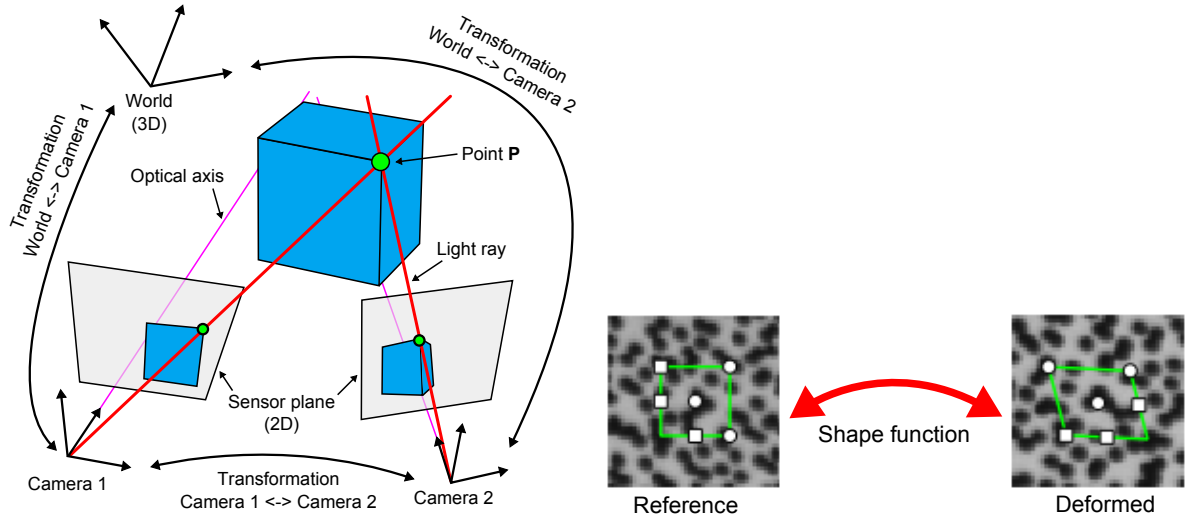

Figure 2. Left: The imaging process for a point $\boldsymbol{P}$ is shown. Here, the front image plane model is used where the sensor plane is assumed in front of the camera to prevent image inversion. Right: The green rectangles are the subsets. The left side shows the subset in the reference image and the right side shows the same subset but in a different image taken from a different perspective.

squared difference criterion (NSSD)

$$\chi^2_{NSSD} = \sum \left(\frac{\sum F_i G_i}{\sum G_i^2} G_i - F_i \right)^2, \tag{2}$$

is used as an optimization criterion to find corresponding subsets in both images. Here, F refers to the pixel values in the reference image, image 1 and G refers to the pixel values in the corresponding image, image 2. The optimization process is normally driven by a Levenberg-Marquardt algorithm [8, 9].

Subsets in the reference image are rectangular. However, corresponding subsets in the following images of the series or from the second camera will most likely not exhibit the same exact rectangular shape (cf. Figure 2 right). This is either due to surface deformation or a change in camera perspective. A shape function is applied to the subset during optimization to estimate possible transformations. Even though, an affine transformation

$$\xi(\boldsymbol{x}, \boldsymbol{p}) = \begin{bmatrix} p_0 \\ p_1 \end{bmatrix} + \begin{bmatrix} 1 + p_2 & p_3 \\ p_4 & 1 + p_5 \end{bmatrix} \boldsymbol{x}, \tag{3}$$

can only approximate the transformation between subsets from different images to a certain level, it is still recommended for small subset sizes [7]. In Eq. 3 $\boldsymbol{x}$ is the vector of a pixel and p_0, p_1, p_2, p_3, p_4, and p_5 are the parameters of the affine transformation. The subset size for correlation is specified in pixels×pixels and each subset corresponds to one test point on the surface under investigation. Subsets can also overlap in order to increase the number of test points on the surface. The degree of overlap is defined by the step size, where a step size of five means that the center of the next subset is shifted by 5 pixels relative to the center of the previous subset.

3. Experimental Setup

This section introduces the experimental setup for the field experiments. The experiments are conducted on a 3.2 MW wind turbine with a rotor diameter of 114 m and a hub height of 93 m [10]. One of the rotor blades is fitted with four areas of random speckle patterns with the help of self adhesive foil. Figure 3 shows an image of the blade taken during one of the experiments. The speckle pattern was applied to the pressure side of the blade on the ground before the rotor was mounted on the wind turbine. The larger black dots on the blade can be used for point tracking and provide several known distances along the blade for calibration and error estimation.

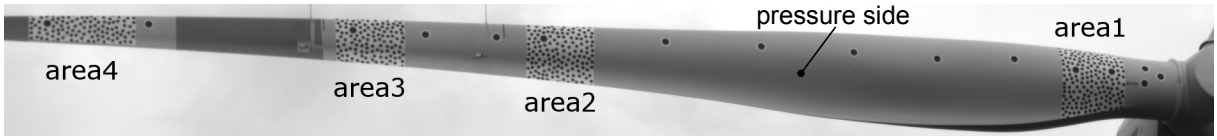

Figure 3. An image of the wind turbine blade with four random speckle patterns attached. This image was taken during one of the experiments with the optical DIC measurement system.

On the left side of Figure 4 the arrangement of the two cameras and the LiDAR around the wind turbine is shown. Depending on the wind direction, the cameras were moved along the white circle (radius = 205 m) and the angle between both cameras was kept at approximately 30°. This corresponds to a distance of approximately 105 m between the cameras. The sampling frequency of the cameras is 30 Hz for every experiment in the present work. The LiDAR was kept at a fixed location for all experiments and did not move if the wind direction changed (cf. Figure 4). On the right of Figure 4, the setup at each of the two camera stations is shown. Each camera station has its own generator, computer, and shelter. The shelter is only used in strong wind to protect the camera because any kind of camera motion or shake must be avoided during image acquisition, otherwise severe errors can arise when the images are processed. A two computer setup was favored over a one computer setup due to the high transfer rate of 750 MBps of each camera. Synchronization of the cameras is achieved with a TTL trigger pulse transmitted via coax cable. This cable is the only connection needed between the two camera stations.

4. Experimental Procedure

In the following subsections, two experiments conducted on the wind turbine during the field-test are presented. In addition, the boundary conditions for the aeroelastic simulations are described and details about the post processing of the results are introduced.

4.1. Data Post Processing

In order to extracted relative and absolute deformations of the blade from the DIC results, it is necessary to eliminate the rigid body rotation of the rotor and the influence of tower and nacelle motion. This is achieved by aligning every recorded position of the blade with an arbitrary chosen reference position. The process of aligning all recorded blade positions is shown in Figure 5 on the right. $T_{n->REF}$ is the translation and $R_{n->REF}$ the corresponding rotation of the rigid body transformation which aligns the current blade position with the reference position. $n = 1, 2, 3, ...$ is the running index or image number of the current blade position. The rigid body transformation is approximated by registering the point cloud of area1 of the current blade position n with the point cloud of area1 of the reference blade position in a least-squares sense. $T_{n->REF}$ and $R_{n->REF}$ are then applied to the complete data-set (area1, area2, area3, and area4) of the current blade position. The point clouds of area1 are chosen for registration because the root of the blade is assumed to be rigid. Once every blade position is transformed to

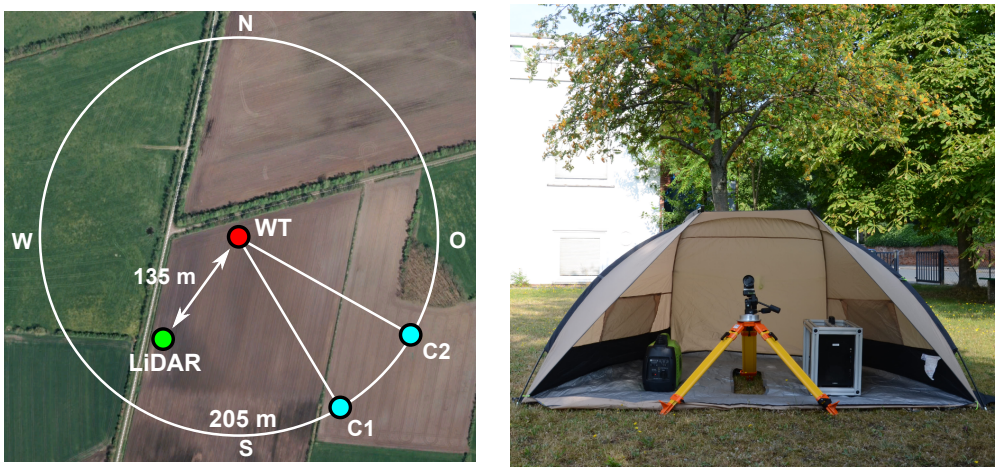

Figure 4. Left: Arrangement of the two cameras (cyan) and the LiDAR (green) around the wind turbine (red); Right: Optical DIC measurment system (only one camera shown)

align with the reference position, the position and orientation of the blade root for every recorded blade position is identical within the limits of the measurement accuracy. However, the position and orientation of area2, area3, and area4 will not be identical due to blade deformation.

The blade deformations measured with DIC are always relative to one reference state of the blade which is defined as having zero deformation. This reference state can be arbitrary chosen from all images in the recorded series. In the present work the reference blade state for all relative deformation measurements corresponds to the blade pointing upwards on the wind turbine. If an unloaded/undeformed reference state of the blade is available in the image series, DIC can also provide absolute deformation data of the blade. The next subsection will explain how a quasi-undeformed reference state of the blade can be realized for DIC measurements on a wind turbine.

4.2. EXP1 - Absolute Deformation

The first experiment (EXP1 - Absolute Deformation) begins with the wind turbine in production mode. After recording approximately 8 rotor rotations, the wind turbine is stopped. With the rotor in idle mode and the blades pitched to feather, the nacelle of the wind turbine is rotated clockwise until both cameras can see the speckle pattern on the pressure side of the blade (cf. Figure 5 left). At this point the wind turbine is kept in idle mode and data acquisition is kept running until the blade with the speckle pattern has passed the tower.

The maneuver of stopping the wind turbine and turning the nacelle by 90° is necessary in order to establish an unloaded/undeformed reference state of the blade. Without this reference state only relative deformations can be measured. However, with this reference state, information about the absolute deformation of the blade become available. In the present study the influence of gravity and wind load acting on the blade pointing downwards is neglected. The blade state, as seen in Figure 5 on the left, where the wind turbine is in idle mode and the nacelle is perpendicular to the incoming wind, is defined as the undeformed reference state. All information about absolute blade deformation for EXP1 are based to this reference at standstill.

4.3. EXP2 - Pitch Angle Step Input Response

The second experiment (EXP2 - Pitch Angle Step Input Response) begins again with the wind turbine in production mode. After recording approximately three rotor rotations, the pitch

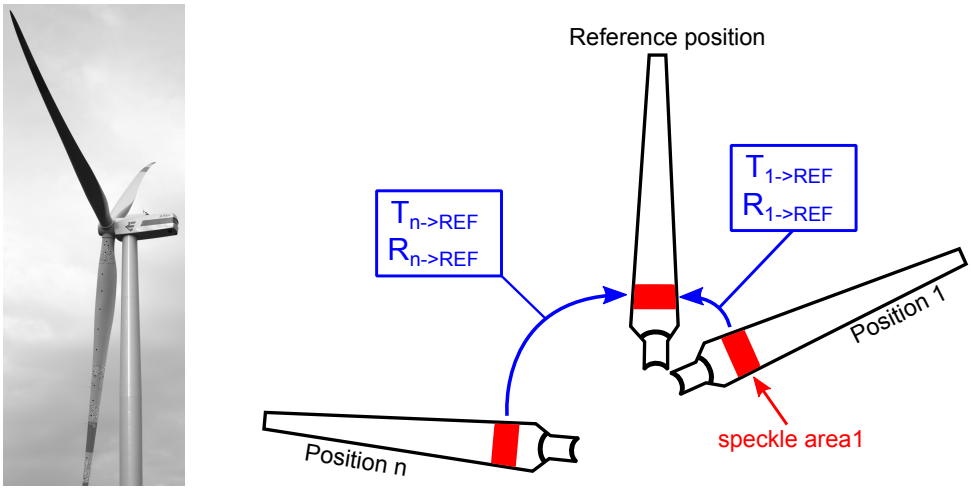

Figure 5. Left: Wind turbine in idle mode with blade pitched to feather as seen by the right camera; Right: Eliminating rotor rotation (Speckle area2, area3, and area4 are not included in the registration process and have been omitted)

angle of all three blades is changed by a step input from 0° to 3° towards feather. Following the pitch step, data acquisition is continued for an additional four rotor rotations.

4.4. Boundary Conditions for Aeroelastic Simulations

The aeroelastic simulations in the present work are based on HAWC2 by DTU Wind Energy. The structural model of the wind turbine is provided by Senvion SE and the 10 min-wind fields for the simulations are generated based on three input parameters:

(i) Average wind speed[1] measured on the nacelle of the wind turbine by means of a cup anemometer during the time of the experiment

(ii) Turbulence intensity based on the wind speed measured on the wind turbine during the time of the experiment

(iii) Wind shear measured by the LiDAR over a period of 10 minutes during the time of the experiment

Figure 6 shows the measured wind speed on the wind turbine for EXP1 and EXP2.

5. Results and Discussion

The following subsections present and discuss the results from EXP1 and EXP2. In addition, the comparison of DIC measurements against aeroelastic simulations is shown and evaluated. In this section, all figures without units on the y-axis are normalized by a consistent factor for out-of-plane and in-plane deflection to maintain comparability. Torsional deflection is normalized by another consistent factor. Both normalization factors are in proximity of the maximum deformation values observed during the experiments. The coordinate system used for data analysis follows the convention recommended by the Germanischer Lloyd [11].

[1] The wind speed data recorded on the nacelle has been corrected to account for the blockage effect of the wind turbine.

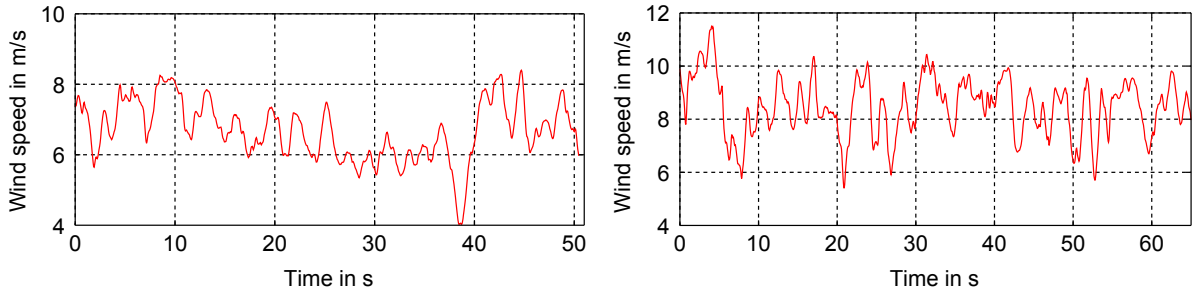

Figure 6. Wind speed on the wind turbine for EXP1 (left) and EXP2 (right) at hub height

5.1. EXP1 - Absolute Deformation

Figure 7 shows the normalized absolute out-of-plane and in-plane deflection and the normalized, relative torsional deformation of the blade for EXP1. On the left side of Figure 7, the data is extracted from area4 at $(z/Z) = 0.87$ spanwise position and on the right side of Figure 7, the data is extracted from area3 at $(z/Z) = 0.65$ spanwise position. A blade position of 0° corresponds to the blade pointing upwards on the wind turbine.

The absolute out-of-plane deflections at area3 and area4 show almost identical characteristics except that absolute and relative amplitudes at area4 are significantly higher. For the first 8 rotations the blade is bend towards the tower while area4 is oscillating around a mean absolute deflection of 0.75 with an amplitude of 0.2 before the wind turbine is shut down and the out-of-plane deflection decreases to zero. The anticipated overshoot of the out-of-plane deflection into the negative region after shutdown is not observed in Figure 7 because the speckle patterns on the blade are already pitched out of sight of the cameras at this time. The observed local minima for the out-of-plane deflections at area4 and area3 appear right after the blade has passed the tower and the observed local maxima are either right at the upright position of the blade or shortly before or after. The location of the local maxima and minima and the direction of bending correspond well to what is expected from aeroelastic simulations and can be attributed to wind shear and the tower shadow effect.

The absolute in-plane deflections at area3 and area4 also show almost identical characteristics except for the absolute and relative amplitudes. The blade is bend towards the leading edge while area4 is oscillating around a mean absolute deflection of -0.35 with an amplitude of 0.18. In addition, the local minima and maxima of the in-plane deflections are observed close to the 90° and 270° rotor position. The location of the local maxima and minima and the direction of bending correspond well to what is expected from aeroelastic simulations and can be explained by gravitational effects.

The relative torsional deflections at area3 and area4 show similar characteristics with the maxima observed shortly before the blade reaches the 12 o'clock position and the minima in proximity to the 6 o'clock position. A very steep rise in torsional deflection is observed after the blade has passed the tower and the peaks at the local maxima appear very sharp when compared to the peaks of the local minima. The descend from the local maxima towards the local minima appears less steep and more gradual. Based on Figure 7, the torsion data at area3 is less susceptible to noise than the torsion data at area4. This is due to the fact that the noise sensitivity of the torsion data does change with the chord length of the blade. Higher chord lengths do improve noise sensitivity and vice versa. An explanation for this observation and a detailed description on how the relative torsion angle is determined based on the DIC data is given in [5]. During shutdown, the optical system records the pitching of the blade up to 30° before the speckle patterns are out of sight of the cameras. However, Figure 7 only shows the

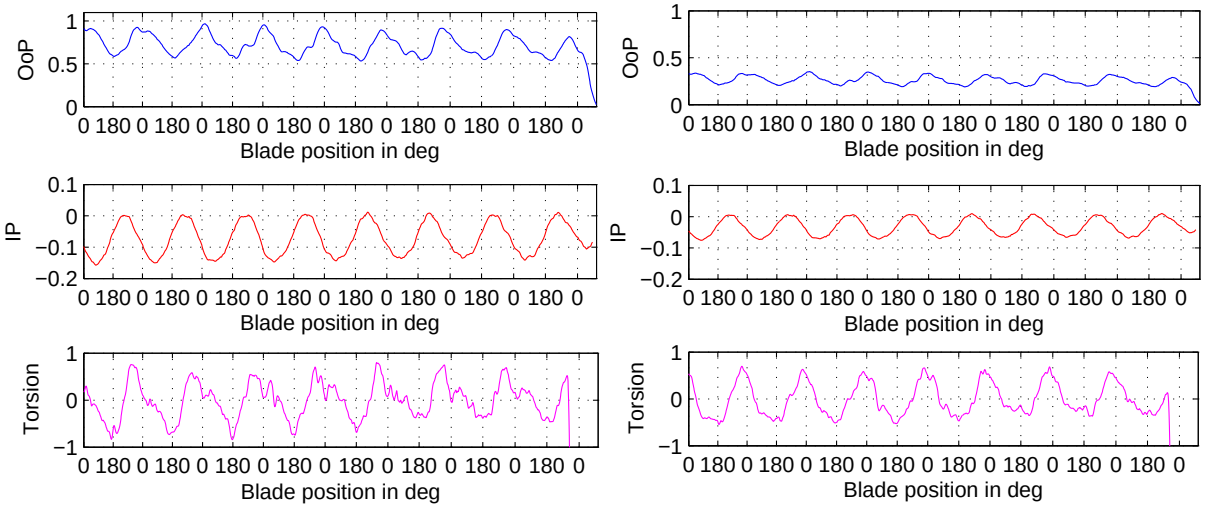

Figure 7. Absolute normalized OoP (out-of-plane) blade deformation, absolute normalized IP (in-plane) blade deformation and relative normalized blade torsion during EXP1 at area4 (left) and area3 (right)

beginning of the pitch motion during shutdown in order to keep the oscillations visible.

It is noted here that the relative torsion angles shown here are very small. The changes in blade deformation necessary to detect these torsion angles are at the very limit of the spatial resolution of the optical system. Therefore, the results should be interpreted with caution until further plausibility checks have been performed.

5.2. EXP2 - Pitch Angle Step Input Response

Figure 8 shows the normalized relative out-of-plane, relative in-plane, and relative torsional deformation of the blade for EXP2. On the left side of Figure 8 the data is extracted from area4 at $(z/Z) = 0.87$ spanwise position and on the right side of Figure 8 the data is extracted from area3 at $(z/Z) = 0.65$ spanwise position. Absolute deformation data is not available for EXP2 because the wind turbine could not be stopped for every experiment (cf. Section 4.2). Since only relative deformations are shown in Figure 8, the data has been adjusted on the y-axis to make the mean relative deformation zero prior to the pitch angle change.

When the pitch angle changes after three rotations, the effect on the out-of-plane deflections is observed with a short time delay. The data at area4 and area3 show a decrease of out-of-plane blade bending shortly after the pitch change occurs. However, the amplitudes of the out-of-plane oscillation around the mean value do not change after the pitch angle change. A similar effect is observed for the in-plane deflections. Here, the in-plane blade bending does decrease once the pitch angle changes, but the amplitudes of the in-plane oscillation around the mean value do not change after the pitch angle change. The observed characteristics for out-of-plane and in-plane bending after a pitch angle step input towards feather correspond well to what is expected from aeroelastic simulations. When the blade is pitched towards feather the loading of the blade decreases and therefore both out-of-plane and in-plane bending must also decrease.

The change in pitch angle is captured very accurate by the relative torsion data. Before and after the change in pitch angle the relative torsion of the blade shows the same characteristics as mentioned before in Section 5.1.

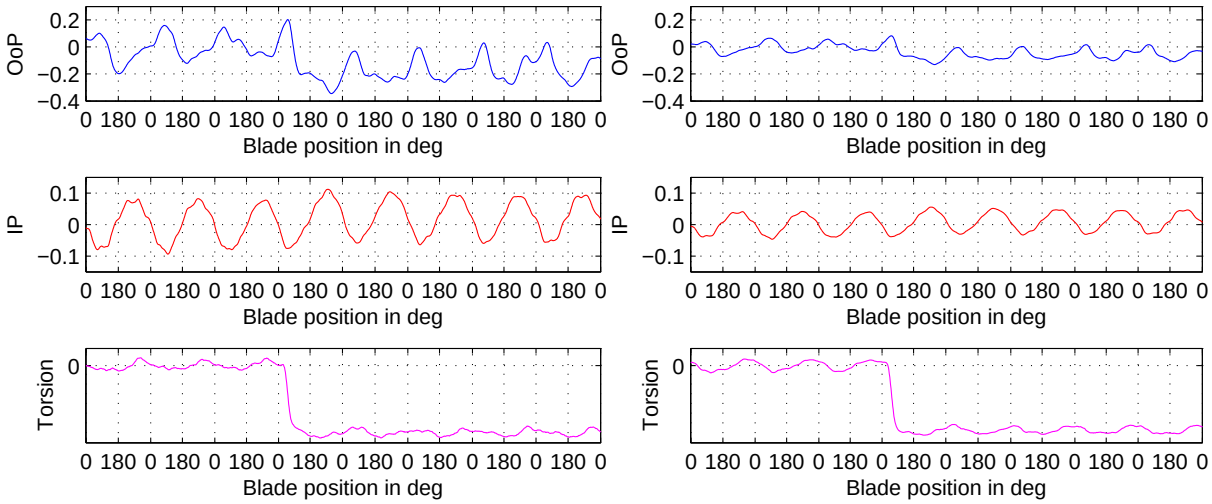

Figure 8. Relative normalized OoP (out-of-plane) blade deformation, relative normalized IP (in-plane) blade deformation and relative normalized blade torsion during EXP2 at area4 (left) and area3 (right)

5.3. DIC Results Compared to Aeroelastic Simulations

The comparison between DIC and aeroelastic simulations for average relative out-of-plane deflection is presented in this subsection. It is based on the results and wind data from EXP1. The following parameters are used to generate the 10-min wind field for the aeroelastic simulation:

- Mean wind speed = 6.7 m/s
- Turbulence intensity = 10 %
- Linear wind shear = 0.0323 (m/s)/m

Within the simulation results a time interval is identified which best matches the wind data and speed curve characteristic of the rotor during EXP1. From this time interval, out-of-plane defection data of one rotor blade is extracted for 8 rotor rotations. In order to make the data from DIC and aeroelastic simulation comparable, the out-of-plane deflection is averaged over the entire 8 rotations and plotted together with the 95% confidence interval. The averaging process is identical for the DIC data and the simulation data. It consists of four stages. First, each entire rotation from 12 o'clock to 12 o'clock position is isolated from the data set. Second, the isolated rotations are shifted along the y-axis until the mean out-of-plane deflection of each rotation equals zero on the y-axis. Third, the isolated rotations are resampled in order to have the same number of samples (360) per rotation. Fourth, the mean and the 95% confidence interval is calculated by averaging over the 8 isolated rotations.

Figure 9 compares the results at area4 on the left side and the results at area3 on the right side. At area4 and area3 the measured and simulated amplitudes compare well and the 95% confidence intervals for DIC and simulation show similar band widths. The minimum out-of-plane deflection measured with DIC is observed right after the blade passes the tower. This minimum corresponds very well with the location of the minimum predicted by the simulation. However, the location of the maximum predicted by the simulation and the location of the maximum measured by DIC is not consistent. The DIC measurements place the maximum shortly before the 12 o'clock position and the simulation predicts the maximum shortly after the 12 o'clock position. This discrepancy

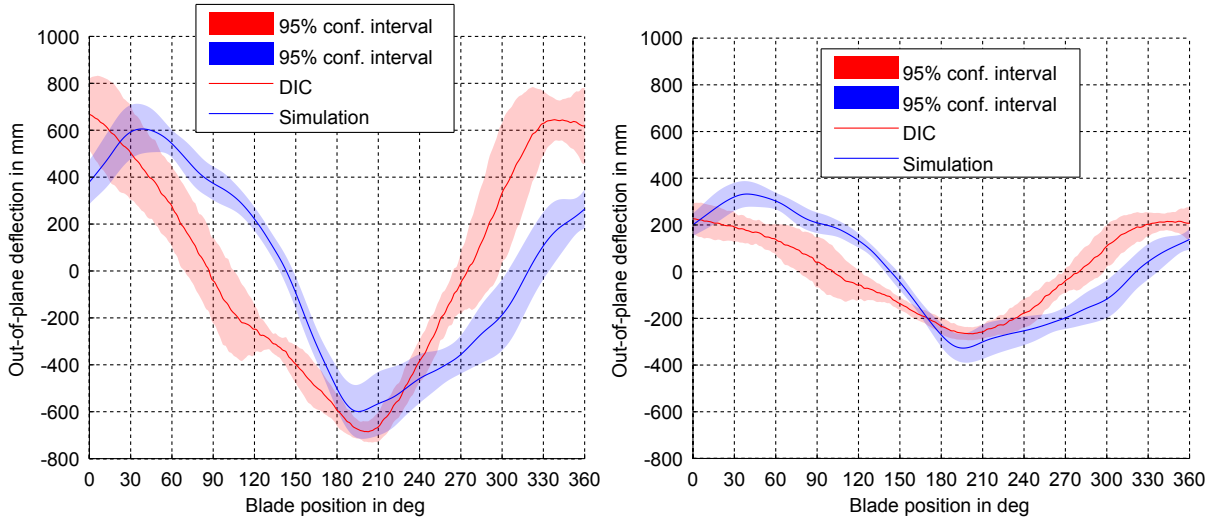

Figure 9. Average relative out-of-plane deflection from DIC compared to average relative out-of-plane deflection from aeroelastic simulation at area4 (left) and area3 (right)

depends mainly on the selected time interval for comparison. From other measurements and simulations it is known that the location of maximum out-of-plane deflection is not as constant as the location of the minimum out-of-plane deflection. In fact, a detailed observation of Figure 7 shows that the location of the maximum can change significantly even for short measurement periods. Therefore, the location of the maximum is highly dependent on the data interval selected for averaging.

6. Conclusions

The present paper evaluates two experiments performed on a 3.2 MW wind turbine and compares the results from one of the experiments to aeroelastic simulations. The intent of these experiments is to demonstrate the feasibility of monitoring wind turbine rotor blades during operation in the interest of design improvements and aeroelastic code validation. Even though only a very limited amount of the available data could be shown here, the results clearly indicate the huge potential that DIC offers for future full-scale wind turbine testing.

The proof of concept shows that DIC is a suitable option for monitoring the absolute and relative, out-of-plane and in-plane deflection, as well as the relative torsion, of a full-scale wind turbine blade during operation. The spatial accuracy of the optical system is high enough to detect even minor changes of blade torsion or a change in out-of-plane and in-plane blade bending after a pitch angle step input. Furthermore, the comparison of relative out-of-plane deflections between simulation and DIC measurements shows good agreement and the differences observed in the location of maximum out-of-plane deflection could be attributed to the selection of the compared data intervals. The comparison demonstrates that data from DIC can be compared to aeroelastic simulations and used for code validation.

Future work will continue with aeroelastic code validation. Here, only relative out-of-plane deflections are compared, but the real challenges are to compare the absolute out-of-plane deformations, include in-plane deformations into the comparison and finally compare also blade torsion angles. Another vital part for thorough code validation is to increase the time length of the data intervals compared. Data series of up to 10 minutes have been recorded during the field test and will be utilized for better statistical significance.

Acknowledgments
The authors gratefully acknowledge the financial funding from the Ministry of Science and Culture of Lower Saxony, Germany. We thank our colleagues here at TFD for the valuable discussions concerning the results of this work. The authors also thank Senvion SE, for granting the opportunity to test the optical DIC measurement system on a full-scale wind turbine.

References

[1] Paulsen U S, Erne O, Moeller T, Sanow G and Schmidt T 2009 *Wind Turbine Operational and Emergency Stop Measurements Using Point Tracking Videogrammetry In Proceedings of the 2009 SEM Annual Conference & Exposition on Experimental & Applied Mechanics*
[2] Ozbek M, Rixen D J, Erne O and Sanow G 2010 *Feasibility of Monitoring Large Wind Turbines using Photogrammetry Energy* **35** 4802 – 4811 ISSN 0360-5442
[3] Ozbek M and Rixen D J 2013 *Operational Modal Analysis of a 2.5 MW Wind Turbine using Optical Measurement Techniques and Strain Gauges Wind Energy* **16** 367–381 ISSN 1099-1824
[4] Winstroth J and Seume J R 2014 *Wind Turbine Rotor Blade Monitoring using Digital Image Correlation: Assessment on a Scaled Model 32nd ASME Wind Energy Symposium*
[5] Winstroth J and Seume J R 2014 *Wind Turbine Rotor Blade Monitoring using Digital Image Correlation: 3D Simulation of the Experimental Setup EWEA 2014*
[6] Triggs B, McLauchlan P F, Hartley R I and Fitzgibbon A W 2000 *Bundle Adjustment - A Modern Synthesis Proceedings of the International Workshop on Vision Algorithms: Theory and Practice* ICCV '99 (Springer) pp 298–372
[7] Sutton M A, Orteu J J and Schreier H 2009 *Image Correlation for Shape, Motion and Deformation Measurements: Basic Concepts,Theory and Applications* (Springer)
[8] Levenberg K 1944 *A method for the solution of certain non-linear problems in least squares Quarterly of Applied Mathematics* **II** 164–168
[9] Marquardt D W 1963 *An algorithm for least-squares estimation of nonlinear parameters SIAM Journal on Applied Mathematics* **11** 431–441
[10] Senvion SE 2014 *Senvion 3.2M114 Datasheet*
[11] Germanischer Lloyd 2010 *Guideline for the Certification of Wind Turbines*